Desalination and Water Treatment
www.deswater.com
doi: 10.1080/19443994.2013.789234

51 (2013) 3662–3674
April

Taylor & Francis
Taylor & Francis Group

A CFD study of heat transfer through spacer channels of membrane distillation modules

M. Shakaib[a,c,*], S.M.F. Hasani[b], M. Ehtesham-ul Haque[c], Iqbal Ahmed[d], R.M. Yunus[a]

[a]*Faculty of Chemical and Natural Resources Engineering, University Malaysia Pahang, Kuantan, Malaysia*
Tel. +92 21 99261261; emails: shakaib@ump.edu.my, mshakaib@live.com
[b]*Department of Mechanical Engineering, Al-Imam Mohammad Ibn Saud Islamic University, Riyadh, Saudi Arabia*
[c]*Department of Mechanical Engineering, NED University of Engineering and Technology, Karachi, Pakistan*
[d]*Chemical Engineering Department, University Technology PETRONAS, Bandar Seri Iskandar, 31750 Tronoh, Perak, Malaysia*

Received 8 September 2012; Accepted 13 March 2013

ABSTRACT

The computational fluid dynamics modeling in this paper examines transient flow and temperature patterns in spacer-filled membrane distillation channels. The instantaneous velocity profiles at various time steps show that at higher Reynolds number the vortices emerge behind spacer filaments, move along with the flow and then finally diminish. This unsteady behavior causes variation in local temperatures and heat transfer coefficients with time. The temperature polarization is usually low near the locations where high velocity region hits the top or attaches to the bottom surface. The region near the filament at the bottom is a stagnant zone and an area of higher temperature polarization at all times. The effect of filament spacing is also investigated. At low Reynolds number and a small filament spacing of 2 mm, maximum values for average shear stress and heat transfer coefficient are obtained. When Reynolds number is high, this spacer becomes unsuitable due to smaller magnitudes of these parameters. The overall analysis shows that the spacers with relatively higher spacing, such as 3 or 4 mm are more appropriate for use in membrane distillation channels.

Keywords: Computational fluid dynamics; Heat transfer coefficient; Membrane distillation; Spacer

1. Introduction

Membrane techniques are widely used for purification of water and other fluids. Based on the mechanism and type of driving force there are popular processes like reverse osmosis, dialysis, gas separation, electrodialysis etc. Among the various processes, membrane distillation (MD) is one that involves temperature/vapor pressure gradient as a driving force for separation. The feed channel in this process consists of hot saline fluid flowing tangentially across a membrane. The permeate channel contains cold fluid, condensing surface with air gap, sweeping gas or vacuum depending on the type of MD configuration [1]. A small portion of the inlet hot feed evaporates due to vapor pressure gradient and

*Corresponding author.

permeates through the membrane. The remaining portion of the feed in aqueous / liquid form is impermeable due to hydrophobic nature of the membrane. The major advantages of MD over other membrane processes are that it rejects almost 100% of ions and macromolecules, requires low operating pressures and membrane materials are chemically less reactive to feed solutions. Another benefit is that it can be coupled with waste or alternative energy sources to yield a cost-effective membrane system [1–3].

A limitation of the MD process which reduces the process effectiveness is temperature polarization phenomenon. Temperature polarization exists due to the fact that the temperature difference across the membrane surfaces $T_{m1} - T_{m2}$ is lower than the difference of the bulk fluid stream temperatures $T_{b1} - T_{b2}$ as shown in Fig. 1. This reduces the driving force for vapor permeation. In MD modules net-type spacers are often used in the flow channels. The spacers disrupt the thermal boundary layer thereby increasing the heat transfer rates and in-turn enhancing the permeate flux.

Various studies have been done related to MD and to investigate the effect of spacers on the membrane performance. Martínez et al. studied the influence of three configurations; open separator, coarse screen separator and fine screen separator [4,5]. It was found that the presence of screen separator (or spacer) results in turbulence due to formation of eddies and wakes, thereby reducing temperature polarization. The study also showed that coarse separator was best among three configurations. In another work Martínez et al. [6] found that increase in feed circulation rates significantly increase the heat transfer coefficients in membrane distillation. Phattaranawik et al. [7] carried out experiments for direct contact membrane distillation. Product flux enhancement of around 31–41% was noticed when spacers were used in the membrane channels. In another paper [8], the same authors considered spacers of different geometries. An optimal spacer was identified with a voidage of 0.6 and a hydrodynamic angle of 90˚. Chernyshov et al. [9] tested spacers with round and twisted filaments for an air-gap MD process. The spacers having round filaments with a flow attack angle of 45˚ and twisted filaments with an angle of 30˚ were found to be more effective. Osman et al. [10] utilized MD process for desalination and concentration of reverse osmosis and electrodialysis brines and showed that water recoveries between 70–80% can be obtained. The treatment of saline water using MD technique was evaluated experimentally by Nghiem et al. [11]. The experiments showed a gradual decline in product flux due to fouling and scaling. Novel designs for the MD process were recently proposed such as vacuum multi-effect MD [12] and solar-powered air gap distillation [13]. Computational fluid dynamics (CFD) has also been applied to study the MD modules. Xu et al. [14] simulated the temperature profiles for air-gap membrane distillation. The results showed that temperature polarization phenomena can be reduced by increasing feed Reynolds number. Alklaibi and Lior [15] performed simulations for three different spacer arrangements: zigzag spacer, non-central suspended and central suspended. The three arrangements were compared on the basis of spacer effectiveness. The central suspended spacer resulted in best performance. The simulation studies of Cipollina et al. [16,17] showed that spacers considerably change the temperature gradients for this process. Sharif et al. [18] used an open source CFD code to model fluid flow and temperature profiles and showed that 3-layer spacer results in lowest pressure drop and symmetrical temperature profile in the membrane channel. Yu et al. [19] found that temperature polarization decreases with the increase in operating temperature. Recently, the present authors modeled steady flow and heat transfer in MD process at various spacer orientations [20]. Some CFD studies [21–26] investigated fluid flow and mass transfer in spacer-filled membrane channels. These studies were focused on nanofiltration/reverse osmosis processes and temperature fields were not obtained. In this paper we study the fluid flow and temperature patterns in a MD process. The spacing between spacer filaments is varied to show that appropriate spacer geometry is important for reducing temperature polarization and to improve the heat transfer characteristics in membrane systems. The MD process, often involve high Reynolds numbers resulting in non-laminar flow, thus causing the velocity and temperature profiles to change with time. This work is therefore extended to include relatively high Reynolds numbers at which flow is unstable and transient.

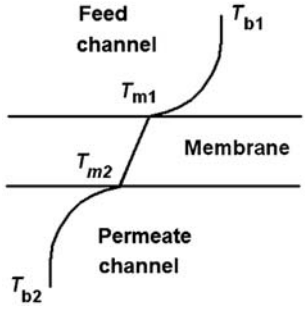

Fig. 1. Temperature profile in membrane distillation.

2. Modeling procedure

Membrane distillation is a complex process in which heat and mass transfer, temperature and concentration polarization and permeation through the membrane are strongly related. The operating temperature of the feed fluid affects the temperature at the membrane surface which in turn varies the permeate flux and also the heat and mass transfer rates in the feed channel. The permeate velocities/fluxes in most of the membrane processes including MD are generally very low when compared to the feed velocities. The water flux in a well-designed MD system is approximately 75 $kg/m^2 h$ [1] which leads to permeate velocity of 2×10^{-5} m/s, considerably lower than the feed velocity. It can therefore be assumed that flow and temperature patterns will not change if permeation is taken into account.

The net-type spacer used in membrane channels contains one set of filaments overlaying on the other set. In flow aligned spacers that contain filaments in longitudinal and transverse directions, the flow characteristics are mainly determined by the transverse filaments while the effect of longitudinal filaments is less significant [27]. Another characteristic of the spacer-filled channel is that it contains a large number of repeating flow cells as shown in Fig. 2. When the permeation velocity is negligible, the flow becomes periodic in nature after overcoming the entrance effects which normally extend to only a few cells. Due to these reasons, it is appropriate to consider a 2D geometry and restrict the computational domain to a single cell rather than modeling the entire channel length (which varies from 0.1–1 m containing hundreds of cells). This procedure significantly reduces the computational time and space. Periodic boundary conditions are used at the opposite vertical faces and mass flow rate is specified in the x-direction. The temperature field in periodic flows is repeating not in the same way as the velocity field because temperatures decrease as fluid flows through the hot channel. The change in temperature and its qualitative profile is however the same at each unit cell [28]. There is a wide range for the inlet temperature used for the feed fluid in the MD system while the heat flux/heat transfer in the system depends on the operating temperature as well as membrane material and porosity, feed flow rate and spacer geometry. To model heat transfer and repeating temperature profiles at various Reynolds number, the bulk fluid temperature (at one of the periodic face) is specified as 330 K whereas heat flux equal to 30 kW/m^2 is applied at the top and the bottom membrane surfaces. The cells are fine enough to yield grid independent solution. For example, 6,000 cells are used for spacer s6 at a Reynolds number of 700. The difference in heat transfer coefficient is less than 1% when compared with 15,000 cells. The governing equations are continuity, momentum and energy equations which are solved using the CFD code FLUENT 6.3. QUICK (Quadratic Upstream Interpolation for Convection Kinetics) scheme is used for discretization of momentum equations whereas Power Law scheme is used for energy equation. Pressure-velocity coupling is made through SIMPLE (Semi-Implicit Method for Pressure Linked Equations) algorithm. For higher Reynolds number flow, simulations are carried out in the unsteady mode with a time step equal to or less than 0.0001 s using second order implicit scheme. Turbulence model is not used as it damps the flow instabilities/unsteady behavior. The viscosity varied with temperature whereas density and thermal conductivity are assumed constant for all the cases. The reason is that the viscosity of many of the fluids (liquids) is a strong function of temperature but the density and the thermal conductivity are not much affected by the temperature variation The geometric characteristics of spacers considered are described in terms of spacing l_m and hydraulic diameter d_h as listed in Table 1. The height of the channel for all spacers is fixed to 1 mm and the width of the computational domain is equal to l_m.

The Reynolds number Re, defined in Eq. (1) is varied from 250–700. The corresponding values of mass flow rate and velocity at periodic faces depend on the type of the spacer/value of hydraulic diameter.

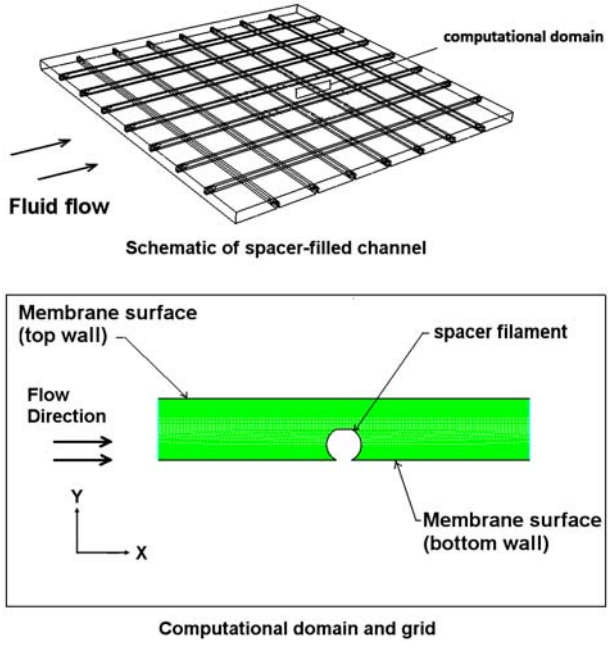

Fig. 2. Schematic and computational domain for spacer-filled channels.

Table 1
Geometric characteristics of spacers

Spacer name	l_m (mm)	d_h (mm)	d_h/l_m
s2	2	1.35	0.675
s3	3	1.53	0.510
s4	4	1.62	0.405
s6	6	1.70	0.283

For example, velocity values are 0.075, 0.125 and 0.2 m/s for spacer s6 at Reynolds number of 260, 440 and 700, respectively.

$$\mathrm{Re} = \frac{u d_h}{v} \tag{1}$$

$$d_h = \frac{4 \times \text{Volume of flow channel}}{\text{Wetted surface area}} \tag{2}$$

In Eq. (1) u is average velocity and v is kinematic viscosity.

Temperature contours in the channel are shown in dimensionless form θ as defined in Eq. (3) due to repeating nature.

$$\theta = \frac{T_l}{T_{max}} \tag{3}$$

In Eq. (3) T_l is local temperature and T_{max} is maximum local temperature.

The spacers are compared on the basis of heat transfer coefficient h:

$$h = \frac{q_w}{T_b - T_m} \tag{4}$$

The effect of Prandtl number is also studied which is defined as:

$$\mathrm{Pr} = \frac{\mu C_p}{k} \tag{5}$$

In Eq. (5) μ is absolute viscosity, C_p is specific heat and k is thermal conductivity. Nusselt number Nu is determined for comparison of present results with ones available in literature. This dimensionless number is:

$$\mathrm{Nu} = \frac{h d_h}{k} \tag{6}$$

The present results are compared with experimental correlations (7) and (8) that were originally developed for mass transfer in various spacer geometries in the Reynolds number range of 100–800 [29,30]. Phattaranawik et al. [7] used Eq. (7) for analysis of the MD process and found satisfactory results due to heat and mass transfer analogy. It therefore, appears reasonable to extend mass transfer correlations for heat transfer in membrane distillation.

$$\mathrm{Nu} = 0.664 \mathrm{Re}^{0.5} \mathrm{Pr}^{0.33} \left(\frac{d_h}{l_m}\right)^{0.5} \tag{7}$$

$$\mathrm{Nu} = 0.664 \mathrm{Re}^{0.875} \mathrm{Pr}^{0.25} \tag{8}$$

3. Results and discussion

The steady velocity and temperature profiles obtained using periodic boundary conditions in spacer s6 at a Reynolds number of 260 are shown in Fig. 3. The velocity profile shows that fluid separates at each filament and results in high velocity zone in the top region. In the bottom region a low velocity zone is formed near the filament which results in a low temperature region. The velocity and temperature contours in other spacers are observed to be similar (not shown here) at this lower value of Reynolds number.

Even though, the simulations in this paper are mainly carried out using periodic conditions with the assumption of impermeability for the membrane surfaces, it is useful to determine velocity and temperature patterns under permeation condition for a few cases. Since permeation cannot be modeled along with periodic boundaries, multiple filaments are created with inlet/outlet boundary conditions and variable heat flux profile. The contours given in Fig. 4 show that velocity profile at the three

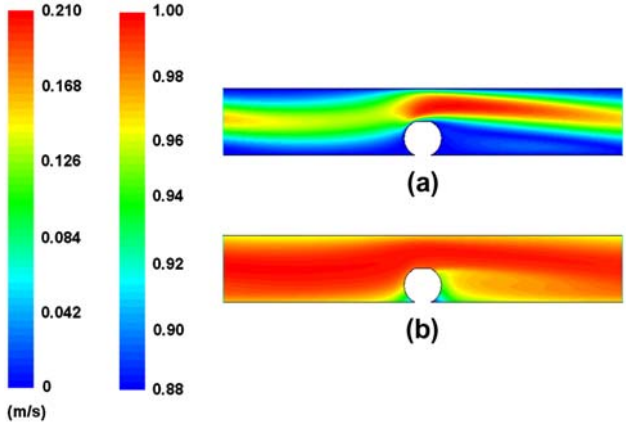

Fig. 3. Contours of (a) velocity and (b) dimensionless temperature in spacer s6 (Re = 260).

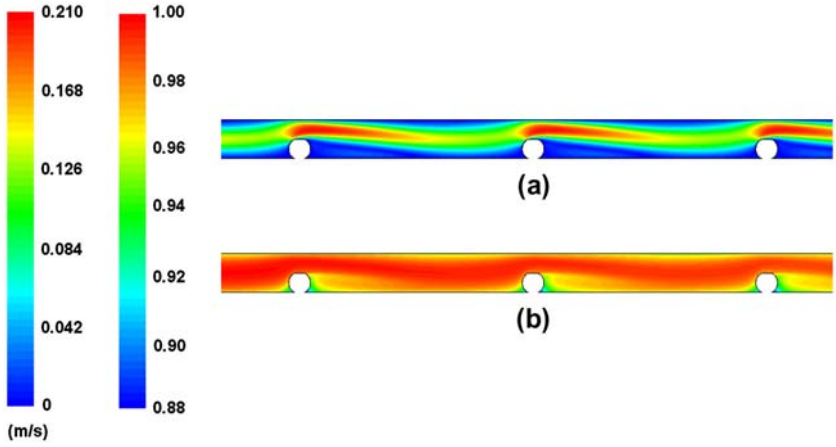

Fig. 4. Contours of (a) velocity and (b) dimensionless temperature in feed channel with multiple filaments at permeate velocity of 2×10^{-5} m/s (spacer s6, Re = 260).

filaments are same. The temperature profile at each filament is of repeating nature, that is, the regions of high and low temperatures are same at each cell indicating a negligible effect of permeate velocity. These findings are consistent with the prior studies [31,32] which showed that low product fluxes do not change the flow behavior in the membrane channels. The variation of local heat transfer coefficient on the top and bottom surface in spacer s6 is shown in Fig. 5. The location $x = 0$ in these plots is the position of filament. The heat transfer is high on the top surface in the central region above the spacer filament ($x \approx 0$) where high velocity region was seen in Fig. 3. On the bottom surface, heat transfer coefficient values increase up to 4,000 W/m^{2}K at $x \approx 0.003$, sharply drop and becomes almost zero near the filament due to stagnant zone. A comparison of heat transfer coefficient without vapor permeation with the heat transfer coefficient with permeation is also shown in Fig. 5. The figure indicates that the plots of heat transfer coefficient using two different modeling approaches are approximately similar.

Performance of a MD system can be affected by the temperatures of the fluids used in the process and the membrane permeation and thermal characteristics. The inlet temperatures are 30–70˚C for the feed solution and 10–40˚C for the permeate solution (in case of direct contact MD process) that result in heat fluxes ranging between 10–70 kW/m^2 as indicated in various studies [4,7,8,33]. Since the effect of membrane is not considered and only the feed side of the system is simulated using periodic boundary conditions, for modeling purpose, fixed values are needed for the inlet bulk temperature T_b and the heat flux q_w. Typical values of T_b and q_w are thus chosen (330 K and

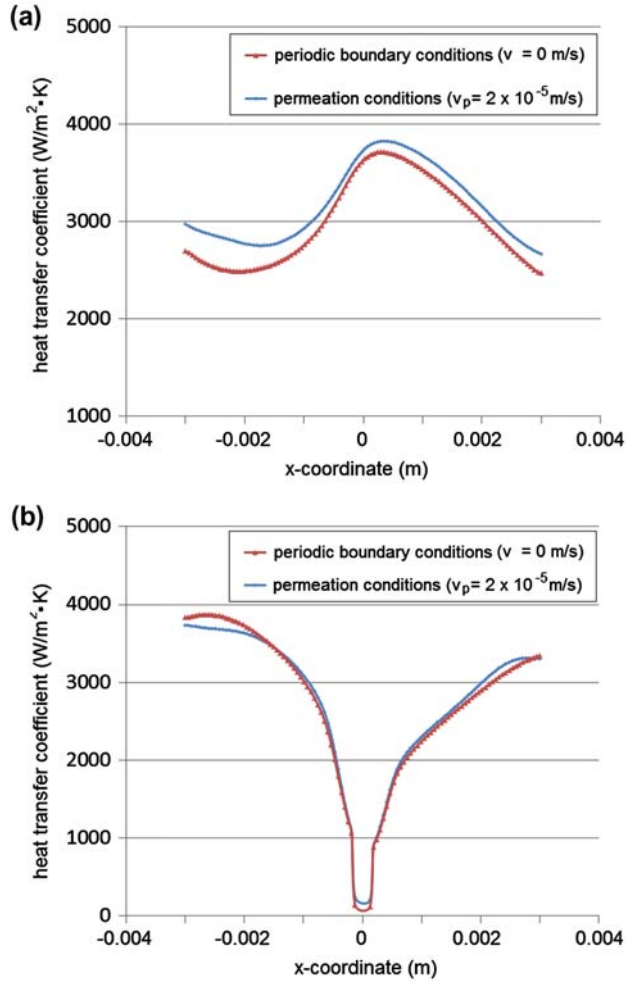

Fig. 5. Heat transfer coefficient at (a) top (b) bottom surface in spacer s6 (Re = 260).

30 kW/m^2, respectively) as mentioned in the Modeling Procedure section. Some results are however obtained

Table 2
Effect of bulk temperature and heat flux on Nusselt number (Re = 260)

	Boundary conditions		
Spacer name	$T_b = 330$ K $q_w = 30$ kW/m^2	$T_b = 330$ K $q_w = 15$ kW/m^2	$T_b = 340$ K $q_w = 30$ kW/m^2
s2	7.706	7.774	7.697
s3	8.560	8.683	8.540
s4	8.112	8.356	8.128
s6	8.468	8.558	8.474

at different bulk fluid temperatures and heat fluxes at the top and the bottom walls and are summarized in Table 2. The Table shows that difference is minor in Nusselt number values determined using different boundary conditions. The reason is that an increase in T_b increases T_m while a decrease in q_w also increases T_m, thus the heat transfer coefficient/Nusselt number (calculated from Eqs. (4) and (6)) is almost same. Though it seems to be a limitation of the simulation procedure that the effect of T_b and q_w on heat transfer coefficient is insignificant, the selected values of 330 K and 30 kW/m^2 can still be considered satisfactory for investigating the unsteady fluid flow and heat transfer in various spacer geometries.

The flow in membrane channels remains fully laminar and steady in the Reynolds number range of 200–400 depending on the spacer geometry [22–24]. At higher Reynolds numbers, the fluid flow is not in pure laminar regime as instabilities appear within the membrane channels due to the presence of spacers, even though the inlet flow rate is set constant with respect to time.

The critical value in spacer-filled channels for such time-dependent flow is 400–800, well below the value for unsteady flow in plane channel. Therefore, when the flow becomes unsteady, smooth high velocity and recirculation regions seen at low Reynolds numbers no longer exist as depicted in Fig. 6. The instantaneous velocity vectors indicate that flow field varies with time and includes continuous formation of multiple vortices that appear, displace and finally disappear. The random flow nature significantly affects the temperature patterns and its profiles are also found to be unsteady as can be noticed in the three time steps of Fig. 6. The temperatures are higher at the location where high velocity fluid strikes the top surface above the filament or reattaches to the bottom surface. At some locations on the top and bottom surfaces, flow separation takes place where the local temperatures become lower. These locations are regions of temperature polarization which is disadvantageous. Due to transient flow structure, however, a desirable aspect is that the locations of some of the low temperature zones change with time indicating periodic disruption of thermal polarization layer. The main recirculation region behind the filament (at the bottom) is an exception in which periodic changes are relatively less and temperature is on the lower side for all time steps. The effect of spacing on unsteady velocity and temperature profiles can be seen in Fig. 7. The vector plot for spacer s3 which has a reduced spacing of 3 mm indicates that an elongated high velocity fluid zone that was observed for spacer s6 does not exist for s3. This zone almost splits into two parts; one above the filament and other somewhere in the center of two filaments. These split high velocity regions change their curvature and continuously attach and detach at the top membrane wall. It can also be inferred from the comparison of unsteady profiles of spacers s3 and s6 that when spacing is large (spacer s6) the vortices appear at one filament, travel freely in the main flow direction and then vanish at the next filament. On the other hand, when spacing is small (spacer s3) the vortices emerge and abruptly die out due to insufficient space to move across the channel. The temperature contours for spacer s3 show some advantageous trends as temperatures do not decrease to very low values behind the filament as was observed for s6.

Due to variation in velocity and temperature contours, the shear stress and heat transfer coefficient also vary in time as shown for top surface in Fig. 8. It is seen in Fig. 8(a), at $t_{ref} = 0$ s for spacer s2, that there are two shear stress peaks; one before the filament ($x \approx -0.0003$) and the other ahead of the filament ($x \approx 0.0007$). The position of these two peaks shift with the passage of time as can be seen in results at $t_{ref} = 0.005$ and 0.01 s. The variation of heat transfer coefficient is a little different as its peak values in most cases are observed to lag behind the shear stress peaks. In spacer s2 ($l_m = 2$ mm), the x-shear stresses are positive at all locations which indicate that flow recirculation does not take place at the top surface. When l_m increases to 3 mm (spacer s3), due to flow separation along with eddies/vortices seen in Fig. 7, shear stress becomes negative at some locations as is clear in Fig. 8(b). When Fig. 8(b) is compared with Fig. 7, it can be noticed that the shear rate is highest at the location where high velocity fluid strikes the top. Similarly the location of negative shear stress is the same as the place where vortices are present. A comparison of Fig. 8(a) and (b) shows that in spacer s3 the magnitudes of shear stress and heat transfer coefficient are higher and their variations with time are more irregular than s2.

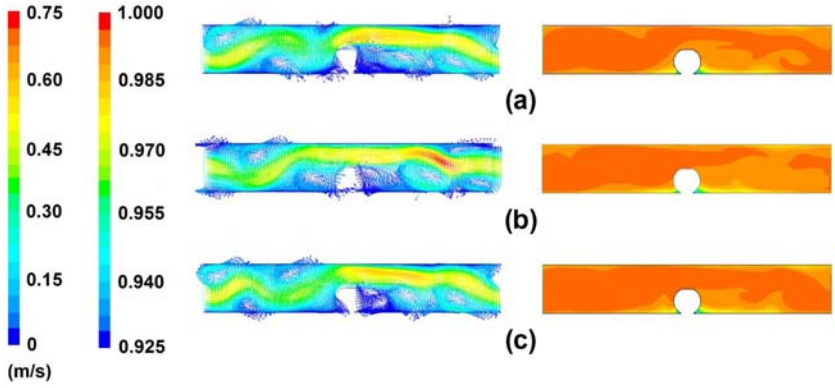

Fig. 6. Velocity vectors and temperature patterns in spacer s6 at Re = 700 at (a) $t_{ref} = 0$ s, (b) $t_{ref} = 0.005$ s, and (c) $t_{ref} = 0.01$ s.

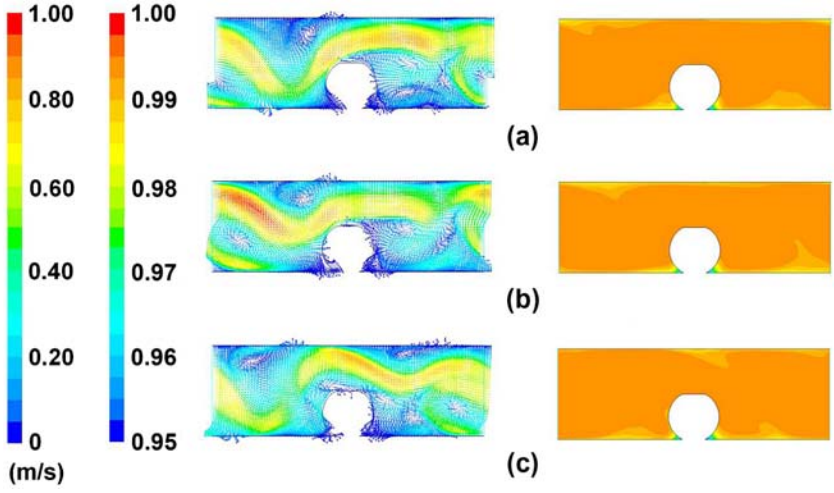

Fig. 7. Velocity vectors and temperature profiles in spacer s3 at Re = 700 at (a) $t_{ref} = 0$ s, (b) $t_{ref} = 0.005$ s, and (c) $t_{ref} = 0.01$ s.

When spacing between filaments is 4 and 6 mm, the variations are again observed to be more prominent in regions $-0.002 < x < -0.0005$ and $-0.003 < x < -0.001$, respectively. The heat transfer coefficient and shear stress on the bottom surface are shown in Fig. 9. In spacer s2, on a major portion, these parameters are very low except at the location ($x = -0.0006$) where negative shear stress and heat transfer coefficient increase up to $2\,N/m^2$ and $13{,}000\,W/m^2K$, respectively. The curves of shear stress and heat transfer coefficient also do not show significant change with time for most of the region. With the increase of spacing the magnitudes as well as the fluctuations of these two variables are noteworthy on a considerable area of the bottom wall. The shear stress is found positive at one instant while negative at the other instant. Both the positive or negative shearing effects have been found to augment the heat transfer coefficient.

The flow instabilities in MD process are also explained with the help of a surface point placed on the top surface as shown in Fig. 10. In spacer s2, the local heat transfer coefficient has a repeating nature with a time period of around 60 steps (or 0.003 s). For larger spacing (s3, s4 and s6) the behavior is of chaotic type at the same Reynolds number of 700. The instantaneous heat transfer coefficients in s3 vary up to 50% from their mean value. In s4 and s6 the deviation is about 25% about the mean. When the Reynolds number is 440, the flow in spacer s2 is steady as evident from its profile which is a straight line. In the other spacers, the randomness observed at Re = 700 is not present at Re = 440. The plots of heat transfer coefficient in s4 and s6 repeat with a period of 200 time steps (0.02 s) while in s3 the repetition occurs approximately after 100 time steps (0.01 s).

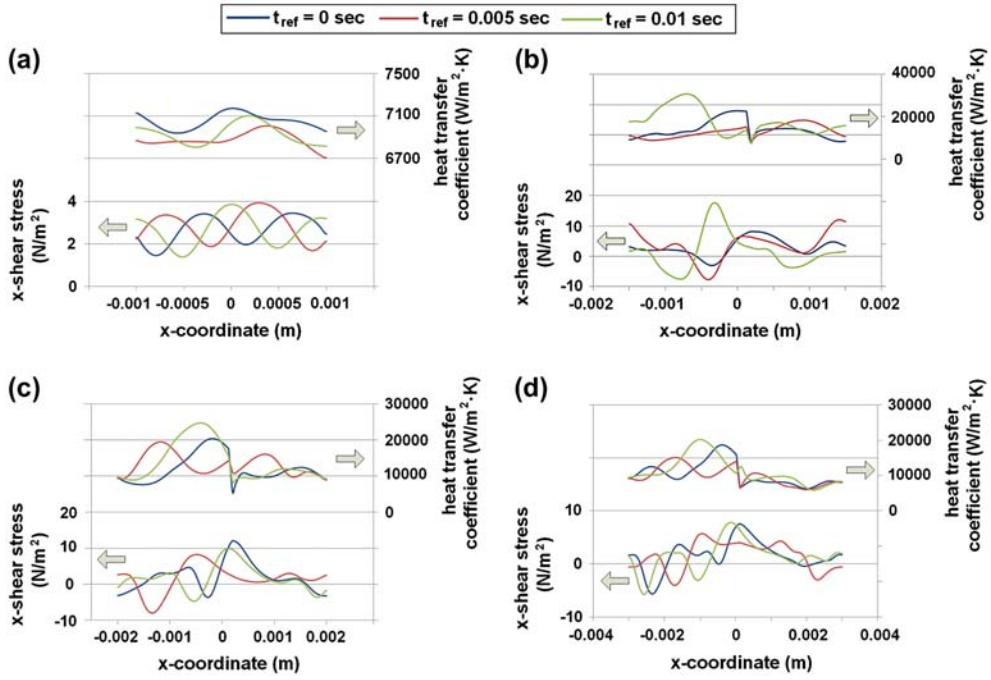

Fig. 8. Variation of shear stress and heat transfer coefficient vs. time in spacer (a) s2, (b) s3, (c) s4, and (d) s6 on top surface.

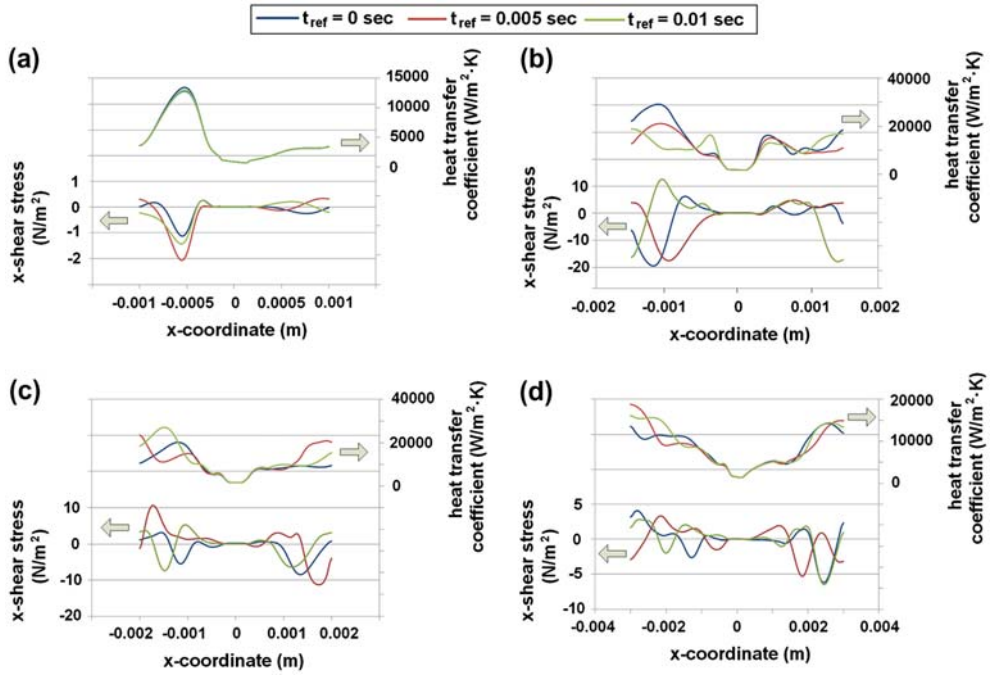

Fig. 9. Shear stress and heat transfer coefficient vs. time in spacer (a) s2 (b) s3 (c) s4 (d) s6 on bottom surface.

The RMS (Root Mean Square) of velocity is shown for the considered spacers in Fig. 11. In spacer s2 the unsteady behavior is less when compared to the other three spacers. In s3 and s4 the velocity fluctuations are higher and increased magnitudes are seen except above the filament where the unsteadiness is lower and in the bottom region very close to the filament, it is almost absent. When the spacing is 6 mm (s6) the unsteadiness is less when compared to s3 or s4. This indicates that the increase in spacing initially increases

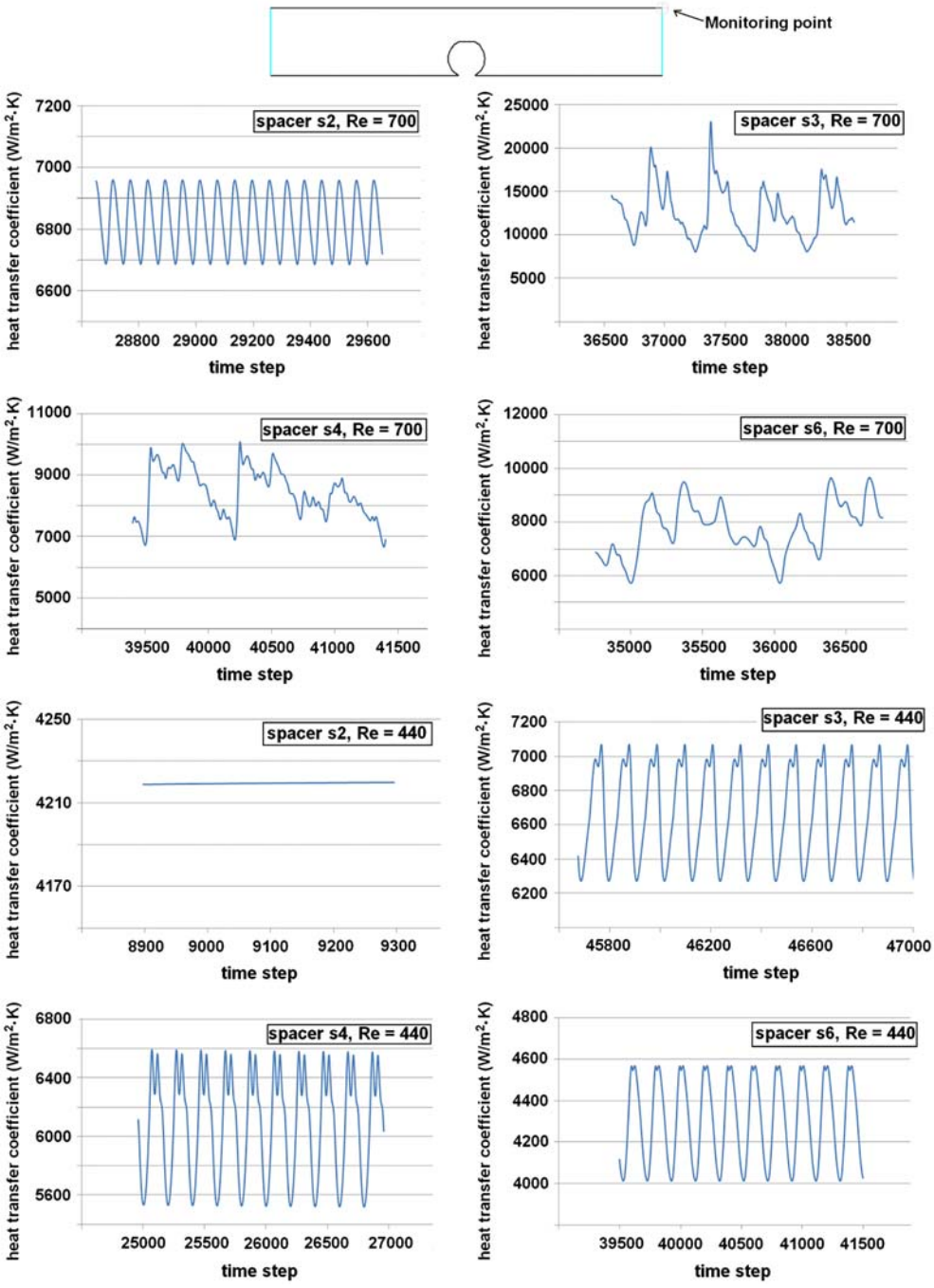

Fig. 10. Heat transfer coefficient at a monitoring point in various spacers.

instabilities in membrane modules and then further increase in spacing decreases the transient behavior.

The four spacers are also compared in terms of average shear stress and heat transfer coefficient. In Fig. 12 it is seen that at low Reynolds numbers the spacer s2 has higher average values of these parameters than the other spacers. When Reynolds number is 440 the spacer s4 has the maximum average value. At Re = 700 spacer s3 becomes superior in performance followed by s4 and then s6. Overall performance of spacers s3 and s4 is better than s2 since at low Reynolds number s2 has only 25% higher shear stress and heat transfer coefficient (than s3 and s4) whereas at higher Reynolds number these parameters in s2 are almost half when compared to s3 or s4. The spacer s6 results in lower shear stress

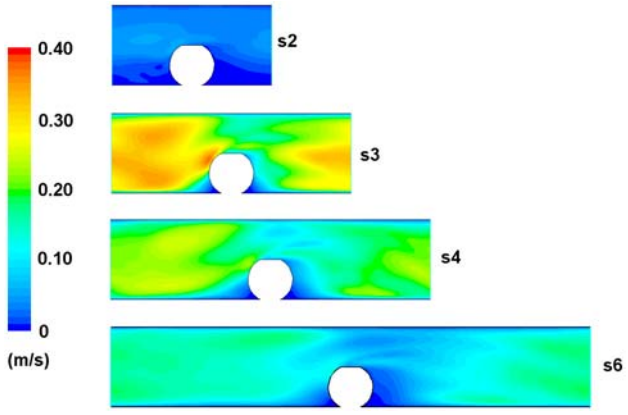

Fig. 11. Contours of velocity fluctuations in the considered spacers (Re = 700).

and heat transfer coefficient for all the considered Reynolds numbers.

The results shown in Figs. 3–12 are at a Prandtl number Pr of 3.7. The membrane processes however are used for a variety of applications like fruit juices concentration and blood purification which involves different Prandtl number values [1].

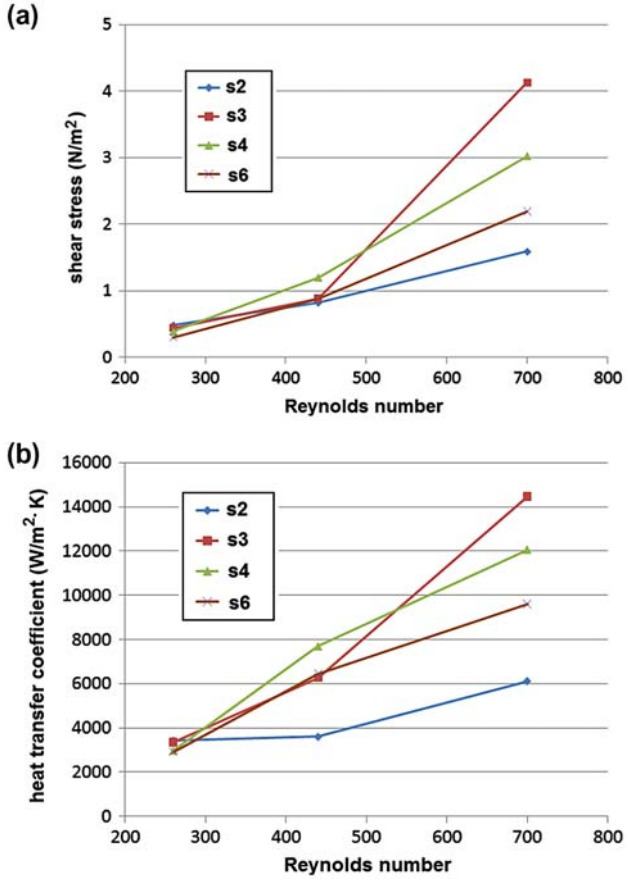

Fig. 12. Average shear stress and heat transfer coefficient.

The effect of Prandtl number for spacer s3 at a Reynolds number of 700 is shown in Fig. 13. As expected, the magnitude of local (time-averaged) heat transfer coefficients on the top and bottom walls is significantly higher when Pr = 3.7. However, the profile is almost similar and location of higher and lower values is the same in both cases. This indicates that increase or decrease in Prandtl number can change the numerical values of heat transfer rates in MD channels but the qualitative results may not be affected much. The average heat transfer coefficients are also determined and it is found that the value is almost half when Pr = 0.7 as compared with Pr = 3.7.

To verify the grid independence of the results, the contours of mean and RMS values of velocity magnitude are obtained and are given in Fig. 14. The contours show that the difference is not significant in patterns of average velocity as well of the velocity fluctuations. The grid can be thus considered acceptable for simulating the transient flow behavior in membrane channels.

From heat transfer coefficients/Nusselt numbers found using the CFD simulation results, a correlation is proposed. The results from the proposed correlation are also compared with the ones obtained using Eqs. (7) and (8). The comparison shown in Fig. 15 shows that in most of the cases the deviations are within ± 60% and ± 40% with Eqs. (7) and (8), respectively. Full agreement between CFD and experimental results cannot be expected due to various approximations and uncertainties imbedded in both methods. For example the spacer filament shape is assumed to be of uniform cross-section for modeling purposes whereas in real spacers the cross-section may not be uniform due to manufacturing defects. Similarly, selection of numerical discretization schemes and assumption of 2D fluid flow in simulations and accuracy of thermocouples used in experiments are the other possible sources of error that can create differences in Nusselt number values at high Reynolds numbers and sometimes also at low Reynolds numbers. Based on the above noted arguments, it is reasonable to say that the differences in results obtained from the two methods are within acceptable limits and conforms to the reliability of this numerical study.

Despite the fact that there is partial agreement in the numerical values of Nusselt numbers obtained from CFD simulations and experiments using Eqs. (7) and (8) as shown in Fig. 15, there are also differences which must be highlighted. In general, Eq. (7) predicts a proportionately increasing behavior of Nusselt number

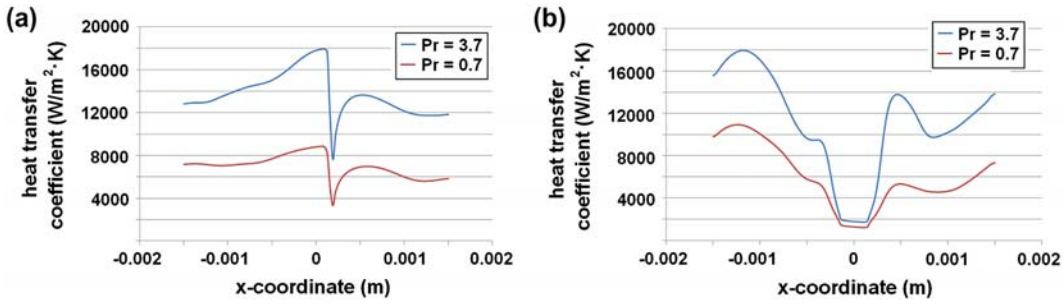

Fig. 13. Effect of Prandtl number on heat transfer coefficient at (a) top (b) bottom surface.

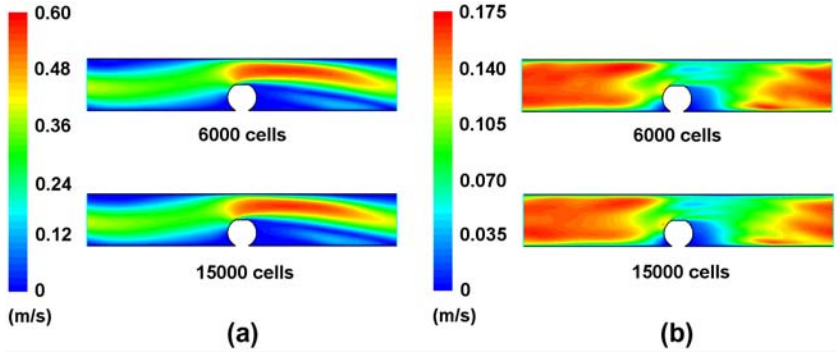

Fig. 14. Contours of (a) mean and (b) RMS velocity magnitude at different grids (spacer s6).

with d_h/l_m ratio, i.e. an increase in d_h/l_m increases Nusselt number Nu. This is not noticed in the present simulation work. In particular for spacer s2 which has higher d_h/l_m but lower Nu due to lower local heat transfer coefficients on a major portion of membrane area (as observed in Figs. 7 and 8). This particular behavior is similar to findings reported in the work of Martinez et al. in which lower heat transfer rates were noticed for a fine separator when compared to a coarse separator [4]. Since the effect of Reynolds number (Re) from CFD simulations is found to be significant on heat transfer, the exponent value 0.875 (for Re), used in Eq. (8) appears reasonable and is therefore retained in the modified correlation given below. Using the CFD results and the experimental correlations, the following modified Eq. (9) is suggested:

$$\mathrm{Nu} = 0.294\mathrm{Re}^{0.875}\mathrm{Pr}^{0.33}\left(\frac{d_h}{l_m}\right)\left(1 - 1.24\frac{d_h}{l_m}\right) \tag{9}$$

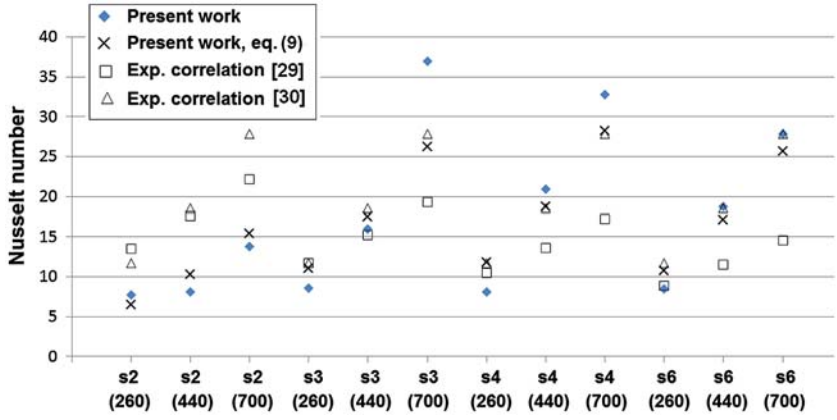

Fig. 15. Comparison of CFD results with experimental correlations (Pr = 3.7).

This correlation satisfactorily predicts the trend of Nusselt number vs. hydraulic diameter/filament spacing ratio. Also the Nusselt number values determined from the developed equation are within ± 20% of the simulated results for the cases considered in this paper.

4. Conclusions

The flow structures and temperature patterns showed great dependence on Reynolds number and filament spacing. For unsteady flows that occurred at higher Reynolds numbers, a number of vortices generated at the bottom surface when the spacing was small. At larger spacing the high velocity zone broke up and separated at the top surface that led to formation of vortices in the top region as well. The RMS contours of velocity indicated that the flow would tend to stabilize when filaments were either very close or very far from each other. When spacing was small the variation of shear stress and heat transfer coefficient occurred only over a limited area but for larger spacing the variation of these parameters with time affected a major portion of the membrane surface. Based on instantaneous plots of shear rates and heat transfer coefficients and their average values, it is expected that spacers with filament spacing between 3–4 mm would provide superior heat transfer characteristics. The simulations at different Prandtl numbers showed that it affected the quantitative values of heat transfer coefficients but the qualitative profile remained the same. The CFD results were also evaluated using an experimental correlation and the comparison showed fair agreement in numerical values of Nusselt number. Based on the simulated results a modified correlation for predicting heat transfer rates in spacer-filled channels was suggested which could predict the simulated results within an accuracy of ± 20%.

Acknowledgements

The support provided by University Malaysia Pahang, Kuantan, Malaysia and NED University of Engineering and Technology, Karachi, Pakistan is acknowledged.

Nomenclature

C_p	—	specific heat (J/kg K)
d_h	—	hydraulic diameter (m)
h	—	heat transfer coefficient (W/m^2 K)
k	—	thermal conductivity (W/m K)
l_m	—	mesh length/filament spacing (m)
Nu	—	Nusselt number
Pr	—	Prandtl number
q_w	—	heat flux (W/m^2)
Re	—	Reynolds number
T_b	—	bulk temperature (K)
T_m	—	temperature at membrane surface (K)
u	—	average velocity (m/s)
μ	—	viscosity (kg/m s)
v	—	kinematic viscosity (m^2/s)

References

[1] K.W. Lawson, D.R. Lloyd, Membrane distillation, J. Membr. Sci. 124 (1997) 1–25.
[2] G.W. Meindersma, C.M. Guijt, A.B. de Haan, Desalination and water recycling by air gap membrane distillation, Desalination 187 (2006) 291–301.
[3] T.Y. Cath, Osmotically and thermally driven membrane processes for enhancement of water recovery in desalination processes, Desalin. Water Treat. 15 (2010) 279–286.
[4] L. Martínez, M.I. Vázquez-González, F.J. Florido-Díaz, Study of membrane distillation using channel spacers, J. Membr. Sci. 144 (1998) 45–56.
[5] L. Martínez, J.M. Rodríguez-Maroto, Characterization of membrane distillation modules and analysis of mass flux enhancement by channel spacers, J. Membr. Sci. 274 (2006) 123–137.
[6] L. Martínez, M.I. Vázquez-González, F.J. Florido-Díaz, Temperature polarization coefficients in membrane distillation, Sep. Sci. Technol. 33 (1998) 787–799.
[7] J. Phattaranawik, R. Jiraratananon, A.G. Fane, C. Halim, Mass flux enhancement using spacer filled channel in direct contact membrane distillation, J. Membr. Sci. 187 (2001) 193–201.
[8] J. Phattaranawik, R. Jiraratananon, A.G. Fane, Effects of net-type spacers on heat and mass transfer in direct contact membrane distillation and comparison with ultrafiltration studies, J. Membr. Sci. 217 (2003) 193–206.
[9] M.N. Chernyshov, G.W. Meindersma, A.B. de Haan, Comparison of spacers for temperature polarization reduction in air gap membrane distillation, Desalination 183 (2005) 363–374.
[10] M.S. Osman, J.J. Schoeman, L.M. Baratta, Desalination/concentration of reverse osmosis and electrodialysis brines with membrane distillation, Desalin. Water Treat. 24 (2010) 293–301.
[11] L.D. Nghiem, F. Hildinger, F.I. Hai, T. Cath, Treatment of saline aqueous solutions using direct contact membrane distillation, Desalin. Water Treat. 32 (2011) 234–241.
[12] W. Heinzl, S. Büttner, G. Lange, Industrialized modules for MED Desalination with polymer surfaces, Desalin. Water Treat. 42 (2012) 177–180.
[13] E.K. Summers, J.H. Lienhard, A novel solar air-gap membrane distillation system, Desalin. Water Treat. 51 (2013) 1344–1351.
[14] Z. Xu, Y. Pan, Y. Yu, CFD simulation on membrane distillation of NaCl solution, Front. Chem. Eng. Chin. 3 (2009) 293–297.
[15] A.M. Alklaibi and N. Lior, Flow modification spacers in membrane distillation (MD) channels, Proceedings of IDA World Congress, Gran Canaria, Spain, (2007).
[16] A. Cipollina, A. Di Miceli, J. Koschikowski, G. Micale, L. Rizzuti, CFD simulation of a membrane distillation module channel, Desalin. Water Treat. 6 (2009) 177–183.
[17] A. Cipollina, G. Micale, L. Rizzuti, Membrane distillation heat transfer enhancement by CFD analysis of internal module geometry, Desalin. Water Treat. 25 (2011) 195–209.
[18] S. Al-Sharif, M. Albeirutty, A. Cipollina, G. Micale, Modelling flow and heat transfer in spacer-filled membrane distillation channels using open source CFD code, Desalination 311 (2013) 103–112.
[19] H. Yu, X. Yang, R. Wang, A.G. Fane, Analysis of heat and mass transfer by CFD for performance enhancement in direct contact membrane distillation, J. Membr. Sci. 405–406 (2012) 38–47.

[20] M. Shakaib, S.M.F. Hasani, I. Ahmed, R.M. Yunus, A CFD study on the effect of spacer orientation on temperature polarization in membrane distillation modules, Desalination 284 (2012) 332–340.
[21] S.M.F. Hasani, M. Shakaib, M. Mahmood, CFD modeling of unsteady fluid flow and mass transfer in spacer-filled membrane modules, Desalin. Water Treat. 9 (2009) 211–220.
[22] J. Schwinge, D.E. Wiley, D.F. Fletcher, Simulation of unsteady flow and vortex shedding for narrow spacer-filled channels, Ind. Eng. Chem. Res. 42 (2003) 4962–4977.
[23] J. Schwinge, D.E. Wiley, D.F. Fletcher, A CFD study of unsteady flow in narrow spacer-filled channels for spiral-wound membrane modules, Desalination 146 (2002) 195–201.
[24] C.P. Koutsou, S.G. Yiantsios, A.J. Karabelas, Numerical simulation of the flow in plane channel containing a periodic array of cylindrical turbulence promoters, J. Membr. Sci. 231 (2004) 81–90.
[25] A.L. Ahmad, K.K. Lau, Impact of different spacer filaments geometries on 2D unsteady hydrodynamics and concentration polarization in spiral wound membrane channel, J. Membr. Sci. 286 (2006) 77–92.
[26] G.A. Fimbres-Weihs, D.E. Wiley, D.F. Fletcher, Unsteady flows with mass transfer in narrow zigzag spacer-filled channels: A numerical study, Ind. Eng. Chem. Res. 45 (2006) 6594–6603.
[27] J.L.C. Santos, V. Geraldes, S. Velizarov, J.G. Crespo, Investigation of flow patterns and mass transfer in membrane module channels filled with flow-aligned spacers using computational fluid dynamics (CFD), J. Membr. Sci. 305 (2007) 103–117.
[28] FLUENT V 6.3, 2006, User's Guide, Fluent Inc., Lebanon, NH.
[29] G. Schock, A. Miquel, Mass transfer and pressure loss in spiral wound modules, Desalination 64 (1987) 339–352.
[30] A.R. Da Costa, A.G. Fane, D.E. Wiley, Spacer characterization and pressure drop modeling in spacer-filled channels, J. Membr. Sci. 87 (1994) 79–98.
[31] M. Shakaib, I. Ahmed, R.M. Yunus, Effect of permeation velocity on flow behavior and pressure drop in feed channels of membranes, Proceedings of ACSSSR Conference on Scientific and Social Science Research, Penang, Malaysia, (2011).
[32] V. Geraldes, V. Semiao, M.N. Pinho, Flow management in nanofiltration spiral wound modules with ladder-type spacers, J. Membr. Sci. 203 (2002) 87–102.
[33] J. Zhang, N. Dow, M. Duke, E. Ostarcevic, J. Li, S. Gray, Identification of material and physical features of membrane distillation membranes for high performance desalination, J. Membr. Sci. 349 (2010) 295–303.